UNVEILING THE ROLE OF α-MnO_2 NANORODS IN BOOSTING ELECTROCHEMICAL PERFORMANCE OF AC–MnO_2 SYMMETRIC SUPERCAPACITORS

Yusril Al Fath*, Surya Prihanto, Ahmad Faruq Abdurrahman, Ayu Aprilia, Suprihatin, Iqbal Firdaus

Department of Physics, Faculty of Mathematics and Natural Sciences, Lampung University, Bandar Lampung, Indonesia

Received: 1st Febraary 2026; Revised: 20th October 2026; Accepted: 30th October 2026

ABSTRACT

Activated carbon (AC) - Manganese dioxide (MnO_2) composite electrodes have attracted significant attention for supercapacitor applications due to the synergistic combination of electric double-layer capacitance from carbon materials and pseudocapacitive charge storage from MnO_2. Despite their promising performance, the influence of MnO_2 morphology on electrochemical behavior remains insufficiently understood when crystal phase and mass loading are controlled. In this work, α-MnO_2 nanorods and α-MnO_2 particles were synthesized via a hydrothermal method and incorporated into AC matrices with identical MnO_2 mass loading to systematically evaluate the effect of morphology on charge-discharge performance. Structural characterization confirms that both materials possess the same α-phase, while distinct one-dimensional and particulate morphologies are observed. Electrochemical measurements show that the nanorod-based composite delivers a superior gravimetric capacitance of 40.67 F g^{-1} and a higher specific energy of 7.36 Wh kg^{-1} compared to the particle-based counterpart. These findings highlight morphology engineering of α-MnO_2 as an effective strategy to further enhance the performance of AC–MnO_2 composite electrodes for supercapacitors.

Keywords: Activated Carbon; α-MnO_2; nanorod; supercapacitor

Introduction

Electricity demand is projected to reach 32,427 TWh by 2030, representing an increase of 4,018 TWh compared to 2024 (28,409 TWh).[1] This trend highlights the growing need for energy storage devices to accommodate rising electricity consumption, one of which is supercapacitors. Supercapacitors are energy storage devices positioned between conventional capacitors and batteries, which exhibit high power density, short charging times, and a long cycle life, making them ideal for long-term applications such as hybrid electric vehicles, electronics, and microgrid storage.[2] The capacitance of a supercapacitor (Electric Double Layer Capacitor, EDLC-type) is primarily generated from the accumulation of electrostatic charges on the surface of porous electrodes when electrolyte ions are adsorbed, forming a stable electrical double layer.

A supercapacitor consists of three main components: electrodes, electrolytes, and separators. In EDLC, activated carbon (AC) serves as the predominant electrode material due to its high electrical conductivity, a large surface area, and high porosity.[3] Despite the superior electrochemical properties of these carbon materials, AC remains the commercial standard owing to its cost-effectiveness. While specific capacitance can be enhanced by increasing surface area, optimizing pore structure, or improving electrolyte wettability, these modifications offer only limited gains. Consequently, significantly increasing specific capacitance often requires hybridizing carbon frameworks with pseudocapacitive materials.[4] MnO_2 holds significant potential as a supercapacitor electrode material due to its advantages over other metal oxides, including reversible redox reactions occurring on the surface of the active

*Corresponding author.
E-Mail: yusril.al@fmipa.unila.ac.id

electrode, high specific capacitance (300–800 F/g), environmental friendliness, low price, and abundance in nature.[5,6] MnO_2 has several crystallographic forms (α, β, γ, and δ), with α-MnO_2 and δ-MnO_2 (birnessite) exhibiting more open structures that enhance ion diffusion and supercapacitive performance. Among these polymorphs, α- MnO_2 is considered the most effective due to its characteristic 2×2 tunnel structure (~0.46 nm) and high surface area.[7,8] Previous studies indicate that 15% MnO_2 loading in AC–MnO_2 optimally enhances electrochemical performance, achieving an approximate 25% increase in capacitance compared to electrodes made of AC electrode.[9,10] Since producing MnO_2 with rapid and reversible surface redox reactions remains challenging, minimizing ion-diffusion lengths at the electrode–electrolyte interface is essential. Nano-sized MnO_2 provides a strategic solution, as its diminished dimensions significantly shorten diffusion pathways compared to bulk counterparts.[11] Given that electrode properties are heavily influenced by particle size, morphology, strain, and synthesis methods, the design of MnO_2 at the nanoscale is critical. Specifically, the morphology, surface area, porosity, and crystalline structure are decisive factors in determining specific capacitance, necessitating the engineering of MnO_2 into optimized nanostructured forms for high-performance supercapacitor applications. For instance, transforming MnO_2 into a nanorod morphology provides a larger specific surface area and more accessible ion pathways, thereby enabling more efficient electrolyte ion penetration and resulting in higher capacitance.[12]

As the development of AC–MnO2 composites continues to evolve, the synergy between the EDLC mechanism of carbon and the pseudocapacitive behavior of MnO_2 has been shown to significantly enhance electrochemical performance. This is particularly evident when MnO_2 is engineered into nanostructured morphologies, such as nanorods, which provide one-dimensional conduction pathways and facilitate efficient ion diffusion. However, although AC-MnO_2 composites have been widely reported, studies that compare different MnO_2 morphologies while keeping the polymorph and mass loading identical remain scarce, so the effect of morphology is often confounded by these two factors.[13] Therefore, this work compares MnO_2 nanorods and particles with the same α-polymorph and identical mass loading in AC–MnO_2 composite electrodes to investigate the influence of MnO_2 morphology on their charge-discharge performance.

Methods

Materials

All chemicals were of analytical grade and used as received without further purification. Activated carbon (AC, CGC, Bangkok, Thailand), carbon black (CB, Imerys, La Hulpe, Belgium), potassium permanganate ($KMnO_4$, purity ≥ 99%), hydrochloric acid (HCl, 37%), sulfuric acid (H_2SO_4, 95-97%), polyvinylidene fluoride (PVDF), and N-methyl-2-pyrrolidone (NMP) were purchased from Merck (Darmstadt, Germany). Tetraethylammonium tetrafluoroborate ($TEABF_4$) was purchased from Gelon, Shandong, China. Deionized (DI) water was obtained from Onelab and used as the solvent throughout the synthesis.

Synthesis of MnO_2

MnO_2 nanorods were synthesized via a hydrothermal method. Briefly, potassium permanganate ($KMnO_4$) and hydrochloric acid (HCl) were dissolved in deionized (DI) water and magnetically stirred for 15 min until a homogeneous purple solution was obtained. The mixture was transferred into a Teflon-lined stainless-steel autoclave and maintained at 140 °C for 8 h. After naturally cooling to room temperature, a dark-brown precipitate was collected and thoroughly washed with ethanol and deionized water four times until the pH reached 6–7. Finally, the obtained MnO_2 product was dried at 60 °C for 24 h.[14]

The AC–MnO_2 particle electrode was prepared following our previous work.[15] In the present work, the electrode was newly characterized by GCD to determine its specific capacitance, specific energy, and specific power. In a typical procedure,

This work is licensed under a Creative Commons Attribution-NonCommercial-ShareAlike 4.0 International License

potassium permanganate powder ($KMnO_4$) and sulfuric acid were dissolved in deionized (DI) water and stirred for 15 minutes until the solution became uniformly purple. The purple solution was transferred to a Teflon-lined autoclave and heated at 120°C for 6 hours. After cooling, a dark brown precipitate was obtained and then washed with ethanol and aquadest four times until the pH reached 6-7. Finally, MnO2 particles were annealed at 60°C for 24 hours.

Fabrication of AC-MnO_2 electrode

The AC-MnO_2 composite slurries, incorporating both MnO_2 particles and nanorods, were prepared using a blending method. The electrode composition consisted of 80 wt% active material AC-MnO_2 (consisting of 65 wt% activated carbon and 15 wt% MnO_2 by total mass), 10 wt% conductive additive (carbon black), and 10 wt% binder polyvinylidene fluoride (PVDF), with MnO_2 accounting for 15 wt% of the active material. Initially, PVDF was dissolved in N-methyl-2-pyrrolidone (NMP) under magnetic stirring at 200 rpm for 30 min until a homogeneous, bubble-free solution was obtained. Subsequently, carbon black, activated carbon, and MnO_2 were gradually added to the solution and continuously stirred for 24 h to achieve a uniform slurry with appropriate viscosity. The resulting composite slurry was then deposited onto aluminum foil substrates to fabricate flexible electrodes. Finally, the AC-MnO_2 electrodes were assembled into a symmetric supercapacitor configuration with a polyethylene membrane as the separator and 1 M TEABF4 as the electrolyte.

Characterization

The crystal structure of each material was analyzed using an X-ray diffractometer (XRD, PANalytical X'Pert PRO, Malvern Panalytical, Worcestershire, UK). The morphologies of the AC, MnO_2, and film electrodes were examined by scanning electron microscopy (SEM, Inspect S50, FEI Company, Hillsboro, OR, USA). The electrochemical performance was evaluated by galvanostatic charge-discharge (GCD) testing using a Neware BTS4000 system (Shenzhen, China) at a current density of 0.1 A g^{-1} within a voltage window of 0-2 V.

Result and Discussion

X-ray diffraction (XRD) analysis was performed to identify the crystalline phases and confirm the successful formation of α-MnO_2. As shown in **Figure 1.a**, the diffraction patterns of both α-MnO_2 particles and nanorods exhibit characteristic reflections that can be well indexed to α-MnO_2 phase and are well matched with the PDF card no. 00-044-0141.[16] The prominent peaks located at $2\theta \approx$ 12.7°, 18.0°, 28.7°, and 37.5°, corresponding to the (110), (200), (310), and (211) planes, respectively, confirm the formation of α-MnO_2. In the AC–MnO_2 composite (**Figure 1.b**), a broad diffraction feature centered at around 23° (002) corresponds to the amorphous nature of activated carbon, while a weak diffraction peak at approximately 12.7° is associated with the (110) plane of α-MnO_2.[17] On the other side, for AC–MnO_2 particles composite **(Figure 1.c)**, MnO_2 reflections appear at 18.01° (200), 28.69° (310), and 37.51° (211**)** from previous work.[15]

The MnO_2 nanorods exhibited an average thickness of 141.69 ± 53 nm and a length of 2.77 ± 0.79 μm (n = 50 nanorods measured using ImageJ), indicaring the formation of one-dimensional MnO_2 structures with aspect ratio of approximately 19 (Figure 2.a). The MnO_2 particles are shown in Figure 2.b. In contrast, the activated carbon morphology shown in Figure 2.c reveals bulk-sized particles with a rough surface texture and numerous apparent surface cavities/voids, which may facilitate electrolyte accessibility and ion transport. The AC–MnO_2 electrode (Figure 3.a) shows MnO_2 nanorods distributed among the activated carbon particles, suggesting the formation of a composite structure. The SEM image suggests good morphological contact between the carbon matrix and the MnO_2 phase.

This morphology may provide favorable pathways for electron and ion transport and may contribute to the electrochemical performance of the composite.[18] However,

This work is licensed under a Creative Commons Attribution-NonCommercial-ShareAlike 4.0 International License

direct confirmation of enhanced electron-transfer behavior would require additional electrochemical characterization. The electrode thickness was measured at 81.03 ± 3.5 μm at 40 different locations (Figure 3.b). The AC–MnO_2 particle electrode (Figure 3.c) shows irregular carbon particles with bright clusters, and its thickness of 79.0 ± 4.6 μm (n = 40, Figure 3d) is comparable to that of the nanorod electrode.

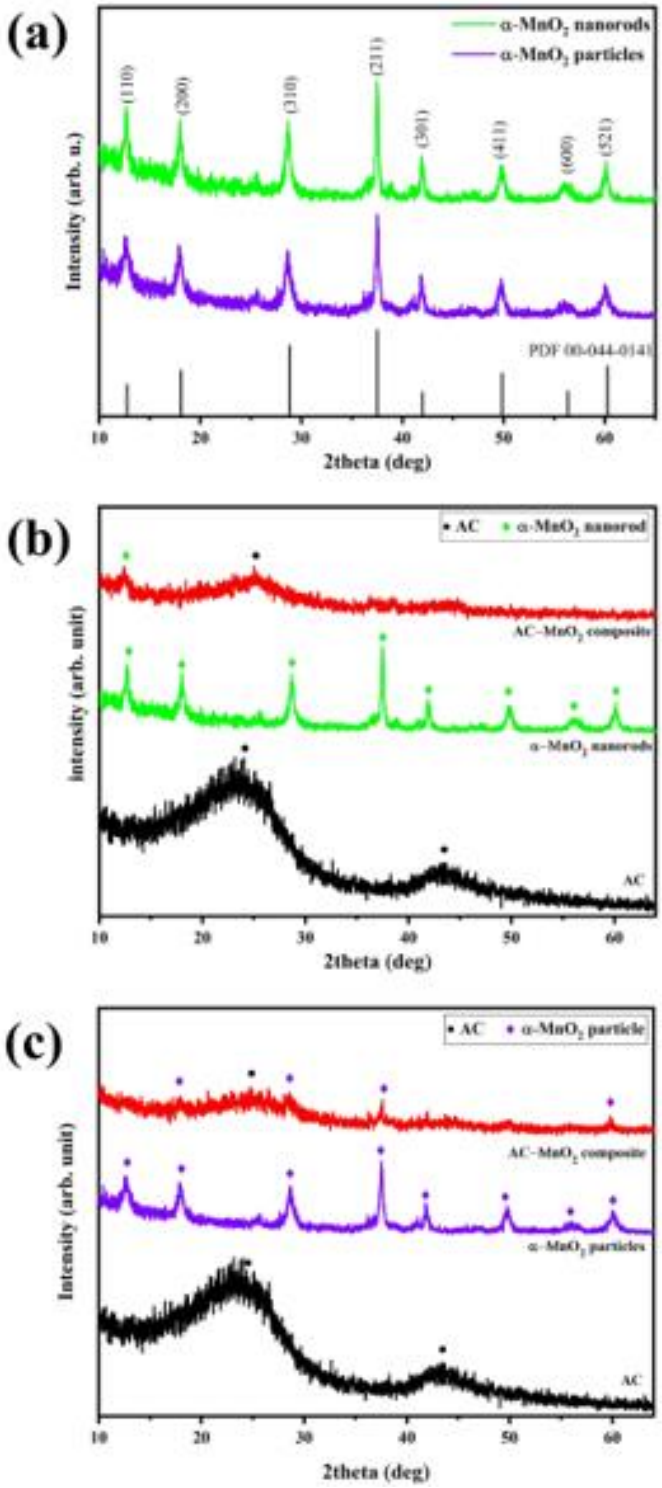


Figure 1. XRD pattern: (a) comparison of α-MnO2 nanorods and particles; (b) AC-MnO_2 nanorods; (c) AC-MnO_2 particles. The XRD data for the particle-based samples in the panels are replotted from the reference.[15]

This work is licensed under a Creative Commons Attribution-NonCommercial-ShareAlike 4.0 International License

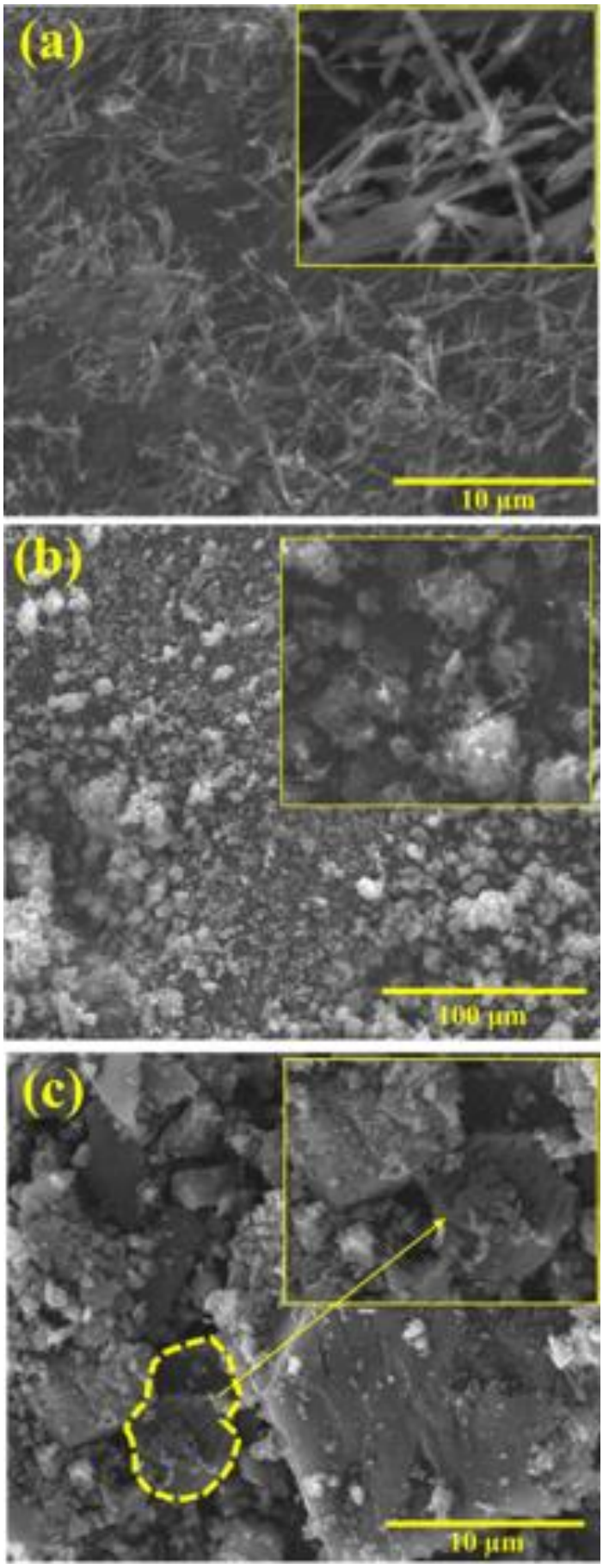


Figure 2. SEM of (a) α-MnO_2 nanorods, (b) α-MnO_2 particles, and (c) Activated Carbon (AC)

This work is licensed under a Creative Commons Attribution-NonCommercial-ShareAlike 4.0 International License

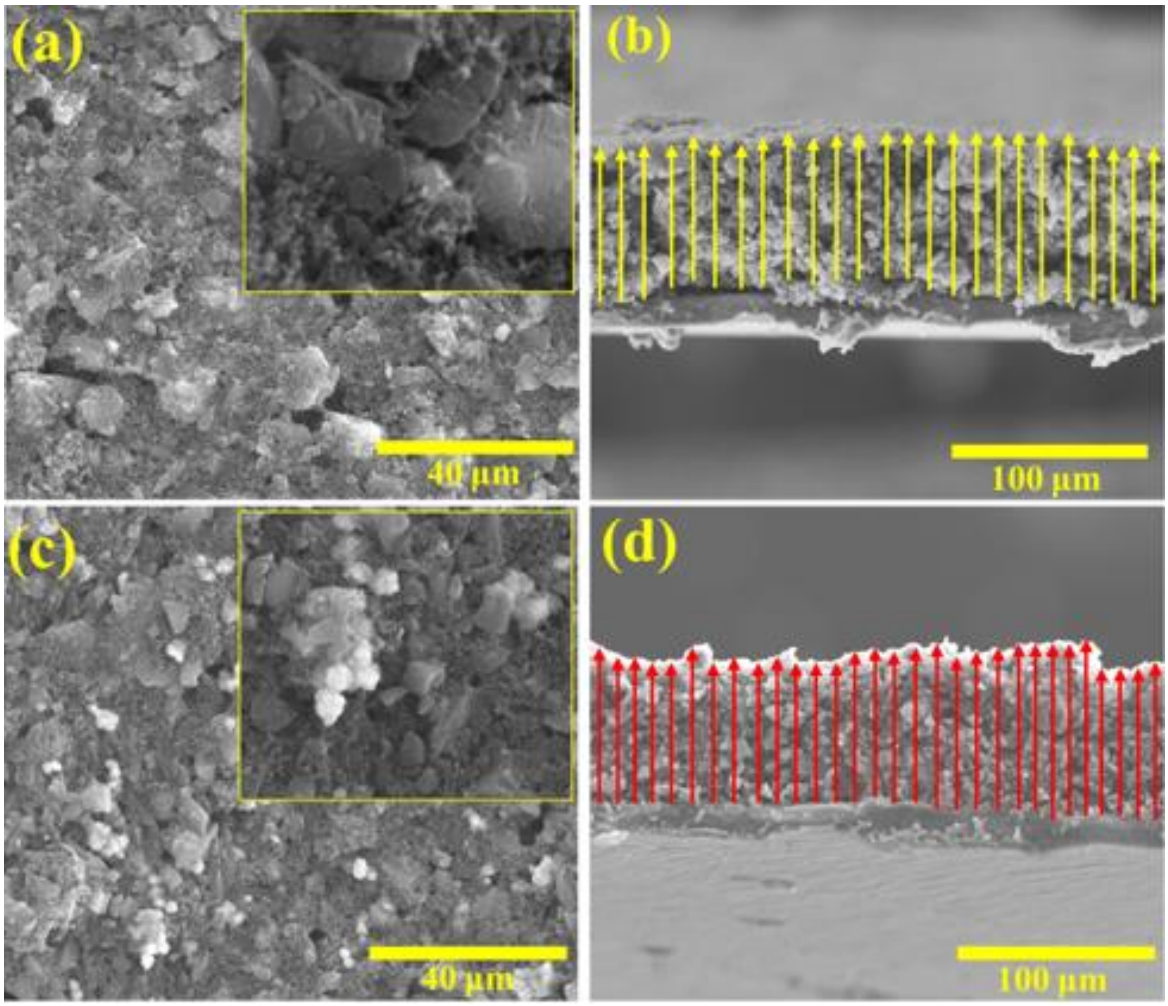


Figure 3. SEM of (a) AC-MnO_2 nanorods, (b) cross-section AC-MnO_2 nanorods, (c) AC-MnO_2 particles, and (d) cross-section AC-MnO_2 particles.

The charge–discharge behavior of the supercapacitor was evaluated using galvanostatic charge–discharge (GCD) measurements. The resulting data consist of voltage (V) as a function of time (t) and were used to determine key electrochemical parameters, including gravimetric specific capacitance (C_s), specific energy (E_s), and specific power (P_s). The equations used to calculate the specific capacitance, specific energy, and specific power are provided in Equations (1)–(3).[19]

$$C_s = \frac{4(I)(\Delta t)}{(m)(\Delta V)} \quad (1)$$

$$E_s = \frac{1}{8}\frac{C_s(\Delta V^2)}{3.6} \quad (2)$$

$$P_s = \frac{E_s \times 3600}{\Delta t} \quad (3)$$

Where m is active mass (g), Δt is total discharge time (s) and ΔV is potential difference during the discharge phase (V).

Table 1 summarizes the comparison of capacitance, specific energy, and specific power between AC–MnO_2 particle and AC–MnO_2 nanorod electrodes. To ensure a fair comparison, both electrodes were prepared with identical MnO_2 mass loading and the same α-MnO_2 crystal phase, indicating that the observed differences in electrochemical performance may originate mainly from morphological effects rather than compositional or phase variations. The AC–MnO_2 nanorod composite exhibits a substantially higher gravimetric capacitance (40.67 F g^{-1}) compared with the AC–MnO_2 particle electrode (13.29 F g^{-1}).

This work is licensed under a Creative Commons Attribution-NonCommercial-ShareAlike 4.0 International License

Table 1. Electrochemical performance of AC with α-MnO_2 nanorods and particles composite

Electrode	Specific Capacitance ($F\ g^{-1}$)	Specific Energy ($Wh\ kg^{-1}$)	Specific Power ($W\ kg^{-1}$)
AC-MnO_2 particles	13.29	4.68	319.12
AC-MnO_2 nanorods	40.67	7.36	228.42

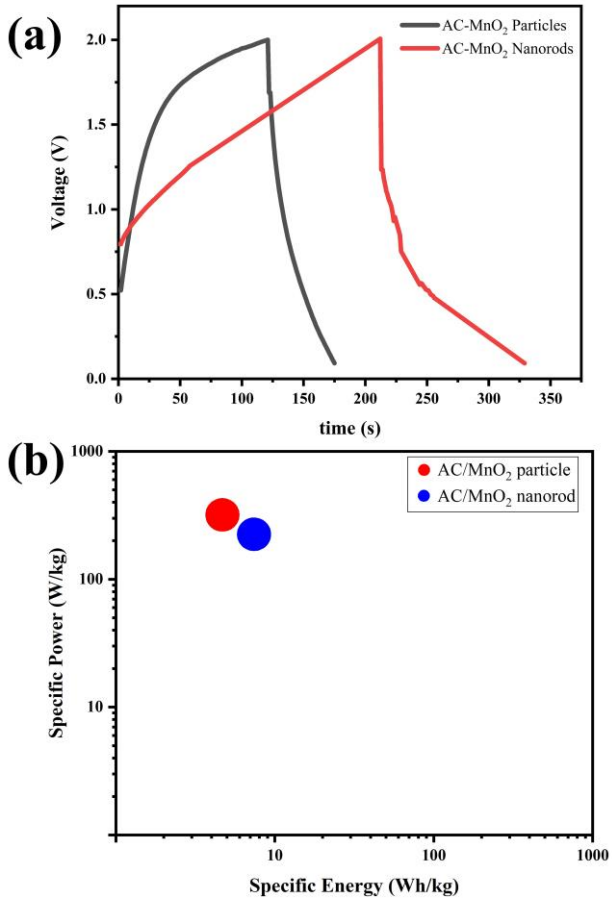


Figure 4. Comparison of AC–MnO_2 particle and AC–MnO_2 nanorod electrodes: (a) galvanostatic charge–discharge (GCD) curves at a current density of 0.1 A g^{-1} and (b) Ragone plot.

The improved electrochemical performance may be associated with the intimate contact between the AC and α-MnO_2 nanorods observed in the SEM images, which could provide more accessible electroactive sites. However, specific surface area and active-site density were not quantitatively determined in this work.[20] In the organic electrolyte (1 M $TEABF_4$), the charge-storage behavior of the AC–MnO_2 composite is expected to be substantially influenced by electric double-layer capacitance associated with the activated-carbon component. The incorporation of MnO_2 may additionally contribute Faradaic or interfacial charge-storage processes, which can influence the deviation of the GCD profiles from an ideal triangular shape. However, further electrochemical analysis is required to quantitatively distinguish the respective EDLC and pseudocapacitive contributions (Figure 4.a).[21] The Ragone plot (Figure 4.b) shows that the AC–MnO_2 nanorod electrode delivers a higher specific energy but a lower specific power than the particle-based electrode. The electrochemical behavior of the composite is primarily influenced by the EDLC contribution of the activated-carbon framework, while the incorporation of nanostructured MnO_2 may introduce additional Faradaic and interfacial charge-storage processes. In the organic electrolyte, the contribution of MnO_2 appears to be limited relative to the dominant carbon-based EDLC

This work is licensed under a Creative Commons Attribution-NonCommercial-ShareAlike 4.0 International License

behavior.[22] These complementary contributions may contribute to the electrochemical performance of the composite, although further quantitative analysis is required to establish the extent of their respective contributions.

The lower capacitance observed for the MnO_2 particle-based electrode may be associated with differences in particle morphology and active-site accessibility. Particle aggregation can potentially reduce the accessible surface area and limit ion transport, which may adversely affect capacitive performance.[23] However, direct morphological characterization would be required to confirm the extent to which agglomeration contributes to the observed difference. The AC–MnO_2 nanorod electrode delivers a higher specific energy of 7.36 Wh kg^{-1} compared with 4.68 Wh kg^{-1} for the particle-based composite. In contrast, the nanorod-based electrode exhibits a lower specific power of 228.42 W kg^{-1} compared with 319.12 W kg^{-1} for the particle-based electrode. This difference indicates a trade-off between energy and power performance under the investigated conditions. The lower power density of the nanorod electrode may be associated with differences in charge-transfer resistance, ion transport, electrode architecture, or other kinetic factors; however, additional electrochemical analysis would be required to identify the dominant mechanism. Overall, under identical MnO_2 phase and mass loading, the nanorod morphology proves more effective than particulate MnO_2 in enhancing charge storage performance, underscoring the importance of morphology engineering in optimizing carbon–MnO_2 composite electrodes for high-performance supercapacitors.

Conclusion

The results indicate that the morphology of α-MnO_2 may play an important role in determining the performance of AC–MnO_2 composite electrodes for supercapacitors. This α-MnO_2 nanorods structural advantage enhances the accessibility of electrochemically active sites and facilitates ion transport, leading to a substantially higher gravimetric capacitance of 40.67 F g^{-1} for the AC–MnO_2 nanorod electrode compared to 13.29 F g^{-1} for the particle-based composite under identical MnO_2 mass loading and crystal phase. The nanorod-based composite delivers an improved specific energy of 7.36 Wh kg^{-1}, surpassing the 4.68 Wh kg^{-1} achieved by the AC–MnO_2 particle electrode. These findings demonstrate that the α-MnO_2 nanorod-based AC–MnO_2 composite exhibits improved electrochemical performance compared with the particle-based composite under the investigated conditions. The results suggest that the use of α-MnO_2 nanorods is a promising approach for improving the performance of AC–MnO_2 composite electrodes for supercapacitor applications. Further morphological and electrochemical characterization is required to clarify the specific contribution of MnO_2 morphology to the observed performance enhancement. Cycling stability should also be evaluated in future work.

Acknowledgement

The authors thank CV Yotta Aksara Energy for providing electrochemical measurement instruments. We also thank Lampung University for supporting this research. The authors declare no conflict of interest.

References

1. Zhang D, Rong C, Ahmad T, Xie H, Zhu H, Li X, et al. Review and outlook of global energy use under the impact of COVID-19. Eng Reports [Internet]. 2023;5(3):e12584. Available from: https://doi.org/10.1002/eng2.12584
2. Asti RD, Putra A. Pengaruh Jenis Larutan Elektrolit Terhadap Sifat Elektrokimia Superkapasitor dari Karbon Aktif Sabut Kelapa Program Studi Kimia , Universitas Negeri Padang. 2024;8:19496–504.
3. Devi R, Kumar V, Kumar S, Kumar Sisodiya A, Kumar Mishra A, Jatrana A, et al. Development of activated carbon by bio waste material for application in supercapacitor electrodes. Mater Lett. 2023 Mar;335:133830.
4. Zhai Z, Zhang L, Du T, Ren B, Xu Y, Wang S, et al. A review of carbon

This work is licensed under a Creative Commons Attribution-NonCommercial-ShareAlike 4.0 International License

materials for supercapacitors. Mater Des [Internet]. 2022;221:111017. Available from: https://doi.org/10.1016/j.matdes.2022.111017
5. Tang XN, Zhu SK, Ning J, Yang XF, Hu MY, Shao JJ. Charge storage mechanisms of manganese dioxide-based supercapacitors: A review. Xinxing Tan Cailiao/New Carbon Mater. 2021;36(4):702–10.
6. Yin M, Miao H, Hu R, Sun Z, Li H. Manganese dioxides for oxygen electrocatalysis in energy conversion and storage systems over full pH range. J Power Sources. 2021;494(March):229779.
7. Jabeen N, Xia Q, Savilov S V, Aldoshin SM, Yu Y, Xia H. Enhanced Pseudocapacitive Performance of α-MnO2 by Cation Preinsertion. ACS Appl Mater Interfaces [Internet]. 2016 Dec 14;8(49):33732–40. Available from: https://doi.org/10.1021/acsami.6b12518
8. Jayachandran M, Rose A, Maiyalagan T, Poongodi N, Vijayakumar T. Effect of various aqueous electrolytes on the electrochemical performance of α-MnO2 nanorods as electrode materials for supercapacitor application. Electrochim Acta. 2021;366:137412.
9. Diantoro M, Istiqomah I, Fath Y Al, Mufti N, Nasikhudin N, Meevasana W, et al. Hierarchical Activated Carbon–MnO2 Composite for Wide Potential Window Asymmetric Supercapacitor Devices in Organic Electrolyte. Micromachines. 2022 Nov;13(11):1989.
10. Al Fath Y, Istiqomah I, Nasikhudin N, Diantoro M, Zulaikah S, Subagio A, et al. Various Low Magnetic Field Effect on Electrochemical Performance of Asymmetric Supercapacitor MnO_2-Carbon-Based Composites. Mater Sci Forum. 2023;1080:99–105.
11. Modungwe TM, Kabongo GL, Mbule PS, Makgopa K, Coetsee E, Dhlamini MS. Unravelling the effect of crystal lattice compression on the supercapacitive performance of hydrothermally grown nanostructured hollandite α-MnO2 induced by incremental growth time. Sci Rep [Internet]. 2024;14(1):25837. Available from: https://doi.org/10.1038/s41598-024-70111-4
12. Liu J, Bao J, Zhang X, Gao Y, Zhang Y, Liu L, et al. MnO2-based materials for supercapacitor electrodes: challenges, strategies and prospects. RSC Adv [Internet]. 2022;12(55):35556–78. Available from: http://dx.doi.org/10.1039/D2RA06664E
13. Diantoro M, Istiqomah I, Fath Y Al, Nasikhudin N, Alias Y, Meevasana W. Potential of MnO2-based composite and numerous morphological for enhancing supercapacitors performance. Int J Appl Ceram Technol. 2023 Jul;20(4):2077–98.
14. Wu J, Huang H, Yu L, Hu J. Controllable Hydrothermal Synthesis of MnO2 Nanostructures. Adv Mater Phys Chem. 2013;03(03):201–5.
15. Diantoro M, Fath Y Al, Mufti N, Saputro A, Pahlevi RA, Muhammad M, et al. Enhancement Ion Diffusion Parameters of Organic Electrolytes on MnO 2 - Carbon Based Supercapacitor Using Low Magnetic Field. J Magentics. 2025;30(2):217–24.
16. Ollegott K, Peters N, Antoni H, Muhler M. Catalytic Carbon Monoxide Oxidation over Potassium-Doped Manganese Dioxide Nanoparticles Synthesized by Spray Drying. Emiss Control Sci Technol [Internet]. 2019;5(4):378–91. Available from: https://doi.org/10.1007/s40825-019-00125-2
17. Fadhil AB, Aziz AM, Altamer MH. Optimization of methyl esters production from non-edible oils using activated carbon supported potassium hydroxide as a solid base catalyst. Arab J Basic Appl Sci [Internet]. 2018;25(2):56–65. Available from: https://doi.org/10.1080/25765299.2018.1449414
18. Kour S, Tanwar S, Sharma AL. MnO2 nanorod loaded activated carbon for high-

This work is licensed under a Creative Commons Attribution-NonCommercial-ShareAlike 4.0 International License

performance supercapacitors. J Alloys Compd [Internet]. 2022;910:164834. Available from: https://doi.org/10.1016/j.jallcom.2022.164834

19. Chen Z, Zhao S, Zhao H, Zou Y, Yu C, Zhong W. Nitrogen-doped interpenetrating porous carbon/graphene networks for supercapacitor applications. Chem Eng J. 2021;409(July 2020):127891.
20. Liu Y, Xiaoxiao Q, Zhang Z, Fan Y, Huang G, Zhang C. MnO2 nanospheres integrated into hierarchical porous carbon as electrode for high performance asymmetrical supercapacitors. J Energy Storage [Internet]. 2023;59:106440. Available from: https://www.sciencedirect.com/science/article/pii/S2352152X2202429X
21. Chodankar NR, Pham HD, Nanjundan AK, Fernando JFS, Jayaramulu K, Golberg D, et al. True Meaning of Pseudocapacitors and Their Performance Metrics: Asymmetric versus Hybrid Supercapacitors. Small. 2020;16(37):1–35.
22. Guan L, Li D, Li Y, Qi C, Iamprasertkun P, Wang B. Sustainable Chemistry for Energy Materials Dimensional engineering of carbon-pseudocapacitive hybrids toward advanced supercapacitors : Recent advances and future perspectives. Sustain Chem Energy Mater [Internet]. 2025;2(September):100022. Available from: https://doi.org/10.1016/j.scenem.2025.100022
23. Plakia L, Kartsonakis IA. A Review on Design, Synthesis and Application of Composite Materials Based on MnO2 for Energy Storage. Vol. 18, Energies. 2025. p. 3455.

This work is licensed under a Creative Commons Attribution-NonCommercial-ShareAlike 4.0 International License